

1 **Estimating the impact of a major hurricane on**
2 **transport processes**

3 Thomas Dobbelaere, Emmanuel Hanert

4 February 15, 2021

5 **Abstract**

6 In most hydrodynamic model studies, currents and waves are simu-
7 lated separately. This is especially true for the simulation of passive
8 drifters, whose trajectories are often computed based solely on cur-
9 rents. Although this simplification holds for most situations, as the
10 force exerted by waves on currents can be neglected in fair weather
11 conditions, it may lead to significant errors in storm conditions, during
12 which local currents are strongly influenced by wind-generated waves.
13 In this study, current-wave interactions in heavy-wind conditions are
14 studied by coupling the unstructured-mesh hydrodynamic model SLIM
15 with the wave model SWAN in the Florida Reef Tract during Hurricane
16 Irma (Sep. 2017). This coupled model successfully reproduced both
17 the observed wave behavior and storm surge during the hurricane.
18 The modeled currents were then used to simulate the trajectories of
19 passive drifters during the passage of the hurricane. Our results show
20 that taking wave force into account induces variations of up 1 m/s
21 in modelled currents on the continental shelf break as well as in the
22 vicinity of reefs and islands. Wave-current interactions can therefore
23 strongly modify the transport of drifting material, such as sediments
24 and coral larvae, during heavy-wind events. That should in particular
25 affect connectivity modeling studies since coral mass spawning events
26 tend to occur during the hurricane season in the Caribbean.

27 **1 Introduction**

28 Individual-based modelling of particulates has been extensively used to
29 study larval connectivity (Figueiredo et al., 2013; Frys et al., 2020) as larval
30 dispersal and demographic connectivity cannot be estimated empirically
31 and genetic similarities are not representative of the flow of individuals re-
32 quired to maintain a population (Cowen and Sponaugle, 2009). In most
33 cases, these models are made up of an ocean model simulating flow features
34 coupled with a Lagrangian tracker including the species-specific life history
35 characteristics and swimming behavior of the particles. Although some of
36 these bio-physical models might account for Stokes drift (Fujimura et al.,
37 2014), wave-induced transport is generally ignored as it is assumed neg-
38 ligible compared to Eulerian currents. Although this assumption holds for
39 fair weather conditions, it is not valid in storm conditions, when wind waves
40 strongly impact currents. Taking storm-induced wave-current interactions
41 into account in coral connectivity studies in Florida might therefore be of
42 outmost importance as hurricanes in this region tend to occur during coral
43 reproduction period (August-September). This was especially true for hur-
44 rricane Irma, that struck the reefs of the Florida Keys in September 2017.
45 As hurricanes intensity and frequency are expected to increase with global
46 warming (REF ?), it is thus critical to assess the impact of wave-induced
47 forces on simulated larval transport in storm conditions and its influence on
48 the predictions of classical individual-based bio-physical models.

- 49 • Damages mostly due to hydrodynamic forces in the Florida Keys (Xian
50 et al., 2018)

51 [TODO: Wave models and wave-current model coupling ?](#)

52 **2 Methods**

53 **2.1 Study area and data**

54 Large-scale ocean circulation around South Florida is dominated by the
55 Florida Current (FC), which originates from the Loop Currents (LC) where it

56 enters the Florida Straits from the Gulf of Mexico, and, downstream, forms
57 the Gulf Stream. The FC is a major western boundary current character-
58 ized by spatial variability and meandering, associated with the presence
59 of cyclonic eddies between the core of the current and the complex reef
60 topography of the Florida Reef Tract (FRT) (Frys et al., 2020; Lee et al.,
61 1995; Kourafalou and Kang, 2012). The northern half of these reefs are
62 made of early Holocene reef frameworks and indurated sand ridges while
63 the southern part (the Florida Keys) is composed of a chain of limestone is-
64 lands, fossilized remnants of ancient coral reefs and sand bars (Hoffmeister
65 and Multer, 1968; Shinn, 1988; Lidz and Shinn, 1991). The variability of the
66 FC extends over a large range of spatial and temporal scales, with periods
67 of 30-70 days in the Lower Keys (Lee et al., 1995) and shorter periods of
68 2-21 days in the Upper Keys (Lee and Mayer, 1977), and exhibits significant
69 seasonal and interannual cycles (Johns and Schott, 1987; Lee and Williams,
70 1988; Schott et al., 1988). Circulation on the West Florida Shelf (WFS) on
71 the other hand is forced by local winds and tidal fluctuations (Lee and Smith,
72 2002; Liu and Weisberg, 2012).

73 Field observations were used to validate our model outputs. Modelled sea
74 surface elevation was validated against tide gauge measurements from
75 the National Oceanic and Atmospheric Administrations (NOAA) Tides and
76 Currents dataset. These measurements were taken at four locations: two
77 in the Florida Keys (Key West and Vaca Key); one on the eastern coast
78 of Florida (Key West); and one on the western coast (Naples). Currents
79 were validated against ADCP measurements from the University of South
80 Florida's College of Marine Science's (USF/CMS) Coastal Ocean Monitoring
81 and Prediction System (COMPS) for the WFS (Weisberg et al., 2009). More
82 specifically, we used measurements from moorings C10, C12 and C13,
83 respectively located at the 25, 50, and 50 m isobaths of the WFS (Liu
84 et al., 2020). Finally, validation of modelled wave parameters was performed
85 against four buoy measurements from NOAA's National Data Buoy Center
86 (NDBC): two on Florida's Eastern shelf and two on the WFS. The locations
87 of all measurement stations are shown on Fig. 1

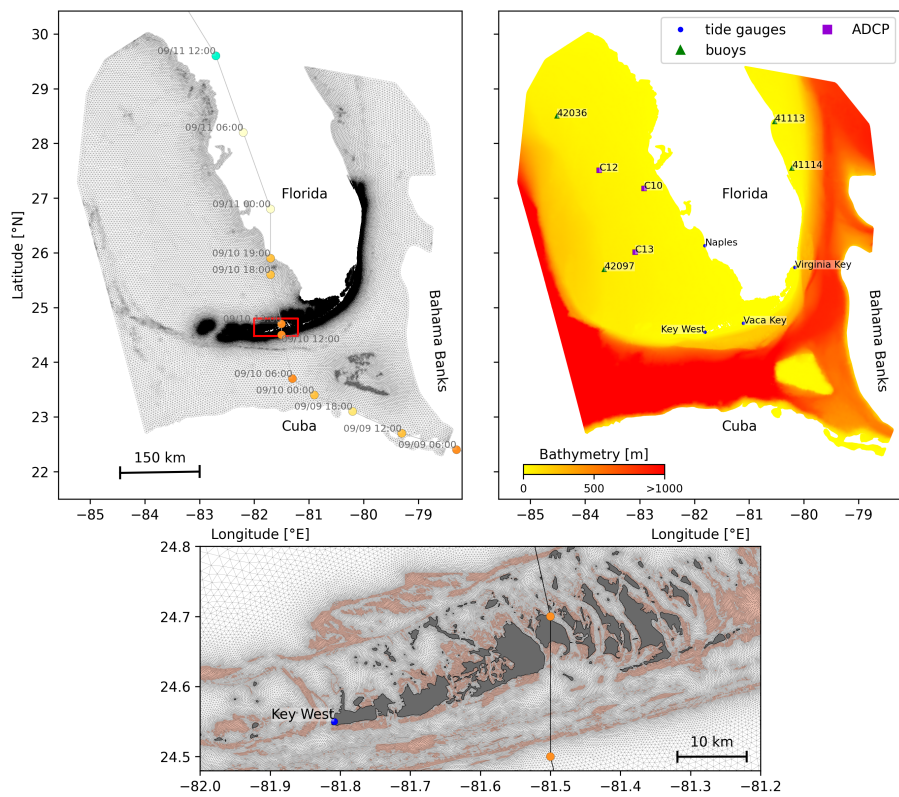


Fig. 1: Upper left: Mesh of the computational domain with the trajectory of Irma, category of the hurricane is given by the Saffir-Simpson color scale. Upper right: Bathymetry of the domain with the location of stations used for the validation of the model outputs. Lower center: Close up view of the 100m mesh resolution near reefs and islands; islands are highlighted in dark grey and coral reefs in coral

88 **2.2 Wind and atmospheric pressure for Hurricane Irma**

89 Irma made landfall in Florida on 10 September 2017 as a category 3 storm,
90 first at Cudjoe Key (Florida Keys) and later on Marco Island, south to Naples
91 (see Fig. 1). It then weakened to a category 2 storm as it moved further
92 inland (Pinelli et al., 2018). The storm caused damages to up to 75% of
93 the buildings at his landfall point in the Florida Keys, making it one of the
94 strongest and costliest hurricanes on record in the Atlantic basin (Xian et al.,
95 2018; Zhang et al., 2019). The strongest reported wind speed was 50 m/s
96 on Marco Island while the highest recorded storm surge was 2.3 m, although
97 larger wind speed occurred in the Florida Keys (Pinelli et al., 2018) In order
98 to reproduce the wind profile of Irma in our model, high-resolution H*Wind
99 (Powell et al., 1998) wind fields were used. As these data represent 1-min
100 averaged wind speeds, we multiplied them by a factor 0.93 to obtain 10-min
101 averaged wind speeds (Harper et al., 2010), more consistent with the time
102 step of our model. Furthermore, H*Wind wind profiles did not cover the whole
103 model extent during the hurricane and were thus blended within coarser
104 wind field extracted from ECMWF ERA-5 datasets. Pressure fields of Irma
105 were also constructed using ERA-5 data. However, the coarse resolution
106 of the data set caused the depression at the center of the hurricane to get
107 smoothed out, leading to an underestimation of the pressure gradient in our
108 model (see eq. 1). To better capture the central depression of Irma, we built
109 a hybrid pressure field using the position and the minimal pressure of the
110 core of the hurricane based on its track in the HURDAT 2 database (Landsea
111 and Franklin, 2013). Based on this information, the hybrid pressure field
112 was constructed by combining an idealized Holland pressure profile (Lin
113 and Chavas, 2012) within the radius of maximum wind speed of Irma (Knaff
114 et al., 2018) with ERA-5 pressure field. The transition between from the
115 Holland profile to ECMWF data outside the radius of maximum wind speed
116 data was performed using a smooth step function.

117 **2.3 Hydrodynamic model**

118 Ocean currents generated during hurricane Irma around South Florida
119 were modelled using the unstructured-mesh depth-integrated coast ocean

120 model SLIM¹. The model mesh covers an area similar to the model extent
 121 of Dobbelaere et al. (2020b), that includes the FRT but also the Florida
 122 Strait and part of the Gulf of Mexico (Figure 1). However, this area has
 123 been slightly extended northeastward and westward in order to include
 124 the location of buoys for wave outputs validation. Furthermore, in order to
 125 withstand potential cell drying due to storm conditions in this study, we used
 126 the conservative mode of SLIM with wetting-drying, whose equations write:

$$\begin{aligned}
 \frac{\partial H}{\partial t} + \nabla \cdot (\mathbf{U}) &= 0 \\
 \frac{\partial \mathbf{U}}{\partial t} + \nabla \cdot \left(\frac{\mathbf{U}\mathbf{U}}{H} \right) &= -f \mathbf{e}_z \times \mathbf{U} + \alpha g H \nabla(H - h) - \frac{1}{\rho} \nabla p_{\text{atm}} + \frac{1}{\rho} \boldsymbol{\tau}_s \quad (1) \\
 &\quad + \nabla \cdot (\nu \nabla \mathbf{U}) - \frac{C_b}{H^2} |\mathbf{U}| \mathbf{U} + \gamma (\mathbf{U}_* - \mathbf{U})
 \end{aligned}$$

127 where H is the water column height and \mathbf{U} is the depth-averaged transport;
 128 f is the Coriolis coefficient; g is the gravitational acceleration; h is the
 129 bathymetry; α is a coefficient stating whether the mesh element is wet
 130 ($\alpha = 1$) or dry ($\alpha = 0$); ν is the viscosity; C_b is the bottom drag coefficient;
 131 ∇p_{atm} is the atmospheric pressure gradient; $\boldsymbol{\tau}_s$ is the surface stress due
 132 to wind; and γ is a relaxation coefficient towards a reference transport \mathbf{U}_* .
 133 As in Frys et al. (2020) and Dobbelaere et al. (2020b), SLIM currents were
 134 relaxed towards HYCOM (Chassignet et al., 2007) in regions where the water
 135 depth exceeds a given threshold. At very high wind speeds, the white cap is
 136 blown off the crest of the waves, which generates a layer of droplets that acts
 137 as a slip layer for the winds at the ocean-atmosphere interface (Holthuijsen
 138 et al., 2012). This causes a saturation of the wind drag coefficient for strong
 139 winds (Donelan et al., 2004; Powell et al., 2003). To account for the impact
 140 of this saturation on the surface wind stress in our model, we implemented
 141 the wind drag parameterization of Moon et al. (2007).

142 The mesh resolution depended on the distance to coastlines and reefs,
 143 bathymetry and bathymetry gradient in order to satisfy SWAN refinement
 144 criterion $h/A \geq a$, where h is the water depth and A is the element area.
 145 The mesh was generated using the Python library seamsh², based on the
 146 the open-source mesh generator GMSH (Geuzaine and Remacle, 2009) and
 147 is composed of approximately 7.7×10^5 elements. The coarsest elements,

¹<https://www.slim-ocean.be>

²<https://pypi.org/project/seamsh/>

¹⁴⁸ far away from the FRT, had a characteristic length size of about 5 km, as
¹⁴⁹ shown in Fig 1 along with the bathymetry of the model domain.

¹⁵⁰ **2.4 Wave model**

¹⁵¹ Waves were modelled using parallel unstructured SWAN (Booij et al., 1999)
¹⁵² on the same mesh as SLIM. This model solves the action balance equation,
¹⁵³ which reads (Mei, 1989):

$$\frac{\partial N}{\partial t} + \nabla_x \cdot [(c_g + \mathbf{u})N] + \frac{\partial}{\partial \theta}[c_\theta N] + \frac{\partial}{\partial \sigma}[c_\sigma N] = \frac{S_{in} + S_{ds} + S_{nl}}{\sigma} \quad (2)$$

¹⁵⁴ where $N = E/\sigma$ is the wave action density; θ is the wave propagation direction;
¹⁵⁵ σ is the wave relative frequency; c_g is the wave group velocity, \mathbf{u} is SLIM
¹⁵⁶ depth-averaged current velocity; c_θ and c_σ are the propagation velocities in
¹⁵⁷ spectral space due to refraction and shifting in frequency due to variations
¹⁵⁸ in depth and currents; and S_{in} , S_{ds} , and S_{nl} respectively represent wave
¹⁵⁹ growth by wind, wave decay and nonlinear transfers of wave energy through
¹⁶⁰ interactions between triplets and quadruplets. Spectra were discretized with
¹⁶¹ 48 direction bins and 50 frequency bins logarithmically distributed from 0.3 to
¹⁶² 2 Hz. Exponential wind growth was parameterized using the formulation of
¹⁶³ Janssen (1991), while dissipations by whitecapping and bottom dissipations
¹⁶⁴ followed the formulations of Komen et al. (1984) and Madsen et al. (1989)
¹⁶⁵ respectively. Coefficients for exponential wind growth and whitecapping
¹⁶⁶ parameterizations were based on the results of Siadatmousavi et al. (2011).
¹⁶⁷ Finally, wave boundary conditions were derived from WAVEWATCH III (Tol-
¹⁶⁸ man et al., 2009) spectral outputs at buoy locations. Depth-averaged Stokes
¹⁶⁹ drift was also computed by SWAN using the following formula:

$$\mathbf{u}_s = \int_0^{2\pi} \int_0^{+\infty} \frac{\sigma^3}{h \tanh(2kh)} E(\sigma, \theta) (\cos \theta, \sin \theta) d\sigma d\theta \quad (3)$$

¹⁷⁰ where k is the norm of the wave vector; h is the water depth; and $E(\sigma, \theta)$ is
¹⁷¹ the wave energy density.

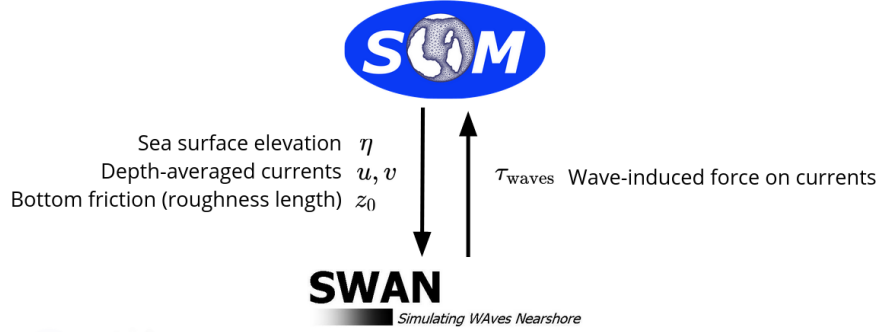


Fig. 2: Schematic illustration of the coupled SLIM+SWAN model.

172 2.5 Coupled model

173 The coupling between SLIM and SWAN is illustrated in Figure 2. The two
 174 models are run consecutively at each time step. First, SLIM computes the
 175 sea surface elevation η and depth-averaged current velocity $\mathbf{u} = (u, v)$.
 176 These quantities are transferred to SWAN to update the model water depth
 177 as well as the second term of equation 2 governing wave energy propagation
 178 in the geographic space. Moreover, in order for the two model to have con-
 179 sistent bottom dissipation parameterizations, SLIM bottom drag coefficient is
 180 transformed into a roughness length z_0 following the methodology of Dietrich
 181 et al. (2011). This roughness length is then converted into Madsen's bottom
 182 dissipation term in SWAN. SWAN then produces the wave-induced force on
 183 current τ_{wave} by computing the wave radiation stress gradient. This quantity
 184 is used to update the value of the surface stress τ_s in equation 1, that now
 185 becomes the sum of wind and wave-induced forces $\tau_s = \tau_{\text{wind}} + \tau_{\text{wave}}$.

186 2.6 Comparison of particle trajectories

187 To assess the impact of the wave coupling on the modelled currents dur-
 188 ing hurricane Irma, we compared the trajectories of virtual particles driven
 189 by currents produced by SLIM alone and SLIM+SWAN simulations in the
 190 Florida Keys. First, we identified the areas where the differences between
 191 the modelled currents were the largest. Then, we determined the potential
 192 origination regions of particles reaching these areas on the passage of the
 193 hurricane through the Florida Keys using backtracking methods (Dobbelaeere

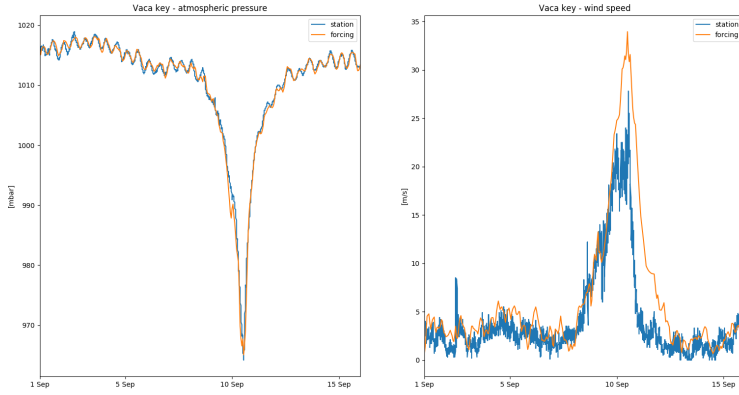


Fig. 3: The atmospheric forcings have been validated with meteorological station observations at Vaca Key. The reconstructed atmospheric pressure and wind speed agree well with field measurements.

et al., 2020a). These regions are highlighted by the 4 release regions of Fig. 7. Finally, particles were released from these four regions and advected by currents produced by the coupled and uncoupled models. At each time step, the center of mass of the modelled particle clouds were computed. The distance between these centers of mass was used as a measure of the impact of the wind-generated wave coupling on the modelled current in the Florida Keys during hurricane Irma. This comparison was performed with 3 sets of currents: the currents modelled by uncoupled SLIM (SLIM); the currents modelled by coupled SLIM+SWAN (SLIM+SWAN); and the SLIM+SWAN currents with depth-averaged Stokes drift (SLIM+SWAN+Stokes).

3 Results

3.1 Validation

Comparisons of the H*Wind wind and hybrid pressure fields with station measurements at Vaca Key are shown in Fig. 3. The observed pressure at the station is well reproduced by the reconstructed hybrid pressure field. H*Wind profile agree well with field measurements as well despite a slight overestimation of the peak wind speed.

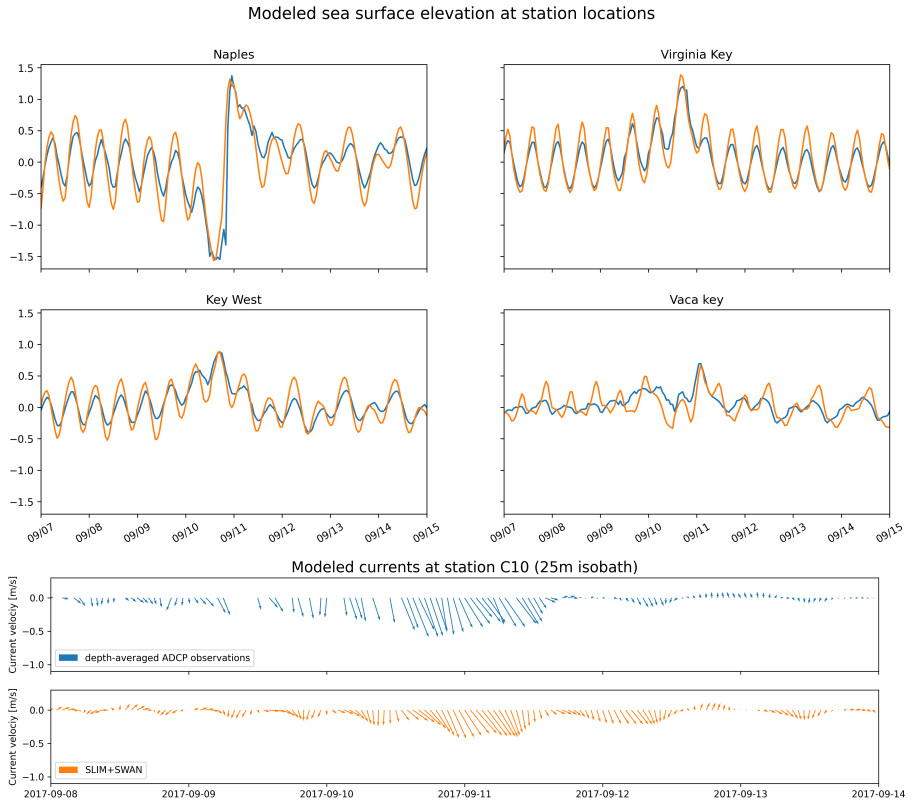


Fig. 4: The sea-surface elevation produced by the coupled wave-current model agrees with SSE and current velocity observations at different stations. The fit is particularly good in the Florida Keys and in Naples, on the inner Florida shelf. The coupled model currents have been validated against current meter data on the inner Florida shelf. The current speed and direction during the hurricane agrees well with the observations.

211 **QUESTION: Should I use quantitative results such as RMSE ?**

212 To validate the hydrodynamic outputs of the coupled wave-current model,
 213 the computed sea surface elevation was compared with tide gauge measure-
 214 ments on the Eastern and Western coasts of Florida as well as in the Florida
 215 Keys. Figure 4 shows a good fit between simulated and measured elevation
 216 at all stations, where the model succeeds in reproducing the observed tide
 217 surge caused by the passage of the Irma. . Measured and modelled depth-
 218 averaged currents at station C10 are shown in Fig. 4. The current speed
 219 and direction during the hurricane agree well with observations.

220 The wave parameters computed by the coupled model were validated

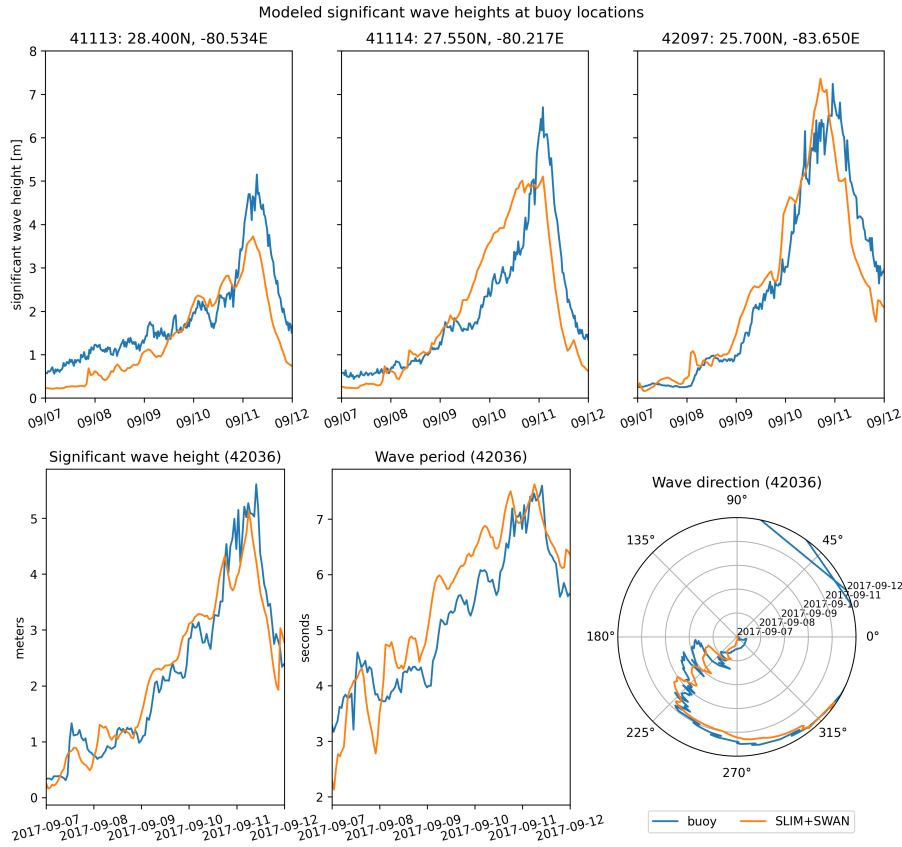


Fig. 5: The significant wave height produced by the coupled model has been compared to buoy measurements at 4 different stations. The timing and amplitude of the peak during the hurricane is correctly reproduced for all stations. For station 42036, the period and direction of the waves also agree well with observations

against field measurements as well. Validation data was extracted from four buoys, two in the Eastern coast Florida and two in the inner shelf. Results of Fig. 5 show that the model reproduces correctly the timing and amplitude of the significant wave height peak during the hurricane for all four stations. Modelled wave period and direction are in good agreement with measurement as well, as shown for station 42036.

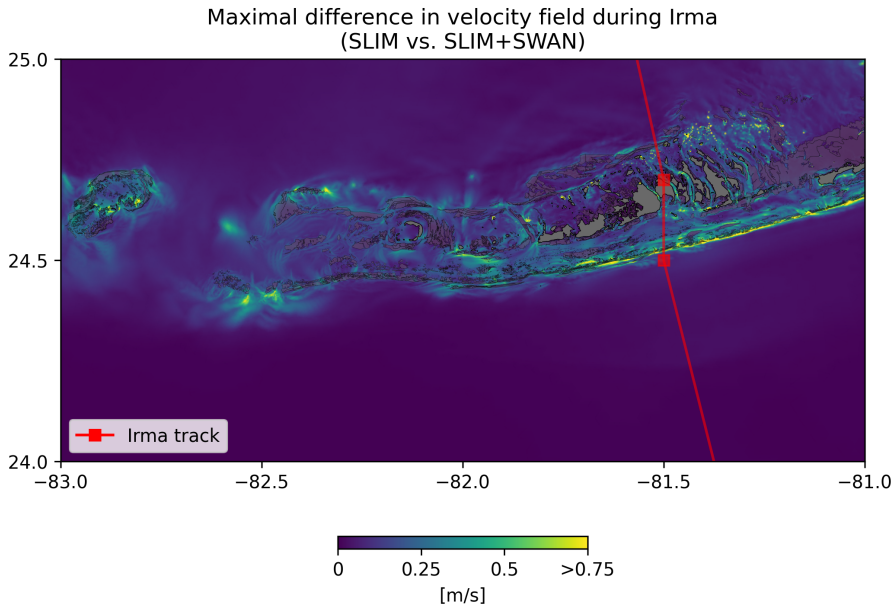


Fig. 6: Maximum of the difference between SLIM and SLIM+SWAN currents speed between 2017-09-07 00:00:00 and 2017-09-13 00:00:00. The difference between the coupled and uncoupled model, which represents the effect of the wave-induced stress, can yield differences of 0.5 m/s in the simulated currents during the passage of the hurricane. SLIM+SWAN currents velocities are larger than the currents modeled by SLIM alone. Islands are highlighted in dark grey and coral reefs in lighter grey

3.2 Impact of waves on currents and transport

The impact of hurricane-induced wave-current interactions is first evaluated by computing the norm of the maximal difference in current velocity between uncoupled SLIM and coupled SLIM+SWAN model runs during the passage of Irma through the Florida Keys (from 2017-09-07 to 2017-09-13). Figure 6 shows that differences in modelled currents are stronger on the shelf break and over coral reefs. These results highlight the significant impact of wave-induced forces, that can yield differences of up to 1 m/s during the hurricane, with stronger currents being obtained with SLIM+SWAN. This suggests that neglecting wave-current interactions during Irma would result in a significant underestimation of transport over reefs.

To quantify the impact of these differences in velocity fields on the modelled trajectories of passive drifters such as coral larvae, we then tracked virtual

240 particles advected by SLIM, SLIM+SWAN and SLIM+SWAN+Stokes cur-
241 rents. Comparison of SLIM and SLIM+SWAN+Stokes trajectories are shown
242 in Fig. 7. Differences between the modelled trajectories are negligible before
243 the passage of the hurricanes in the Florida Keys. Then, distance between
244 the centers of mass of the particles abruptly increase to up to tens of kilo-
245 meters as Irma gets through the Keys to finally stabilize after the passage
246 of the hurricane. These results support the assumption that wave-induced
247 transport is negligible compared to advection by Eulerian currents in fair
248 whether conditions. However, ignoring waves in storm conditions could
249 result in significant inaccuracies in modelled trajectories, as illustrated in
250 the case of release region 2 in Fig. 7. Particles advected by the currents
251 of the coupled model tend to remain on the shelf while particles advected
252 by SLIM alone are mostly transported along the shelf break. Although not
253 shown in this paper, comparison of SLIM and SLIM+SWAN trajectories were
254 conducted as well. The evolution of the distance between centers of mass
255 of the particle clouds showed similar trends while yielding smaller values.
256 Modelled maximal depth-averaged Stokes drift reached up to 0.2 m/s during
257 the passage of Irma through the Florida Keys. This suggests that both the
258 impact of wave-induced force on Eulerian currents and Stokes drift should be
259 taken into account while modelling particle transport under storm conditions.

260 4 Discussion and conclusions

- 261 Impact of waves on coral connectivity
262 Ability of wave model to correctly capture gradient in significant wave height
263 due to current-waves interactions under tropical cyclones depends on:
- 264 • Spatial (10km → 5km) and spectral (36 dir. → 48 dir.) resolution
265 (Hegermiller et al., 2019)
 - 266 • Directional spreading of incident waves (Villas Bôas et al., 2020)

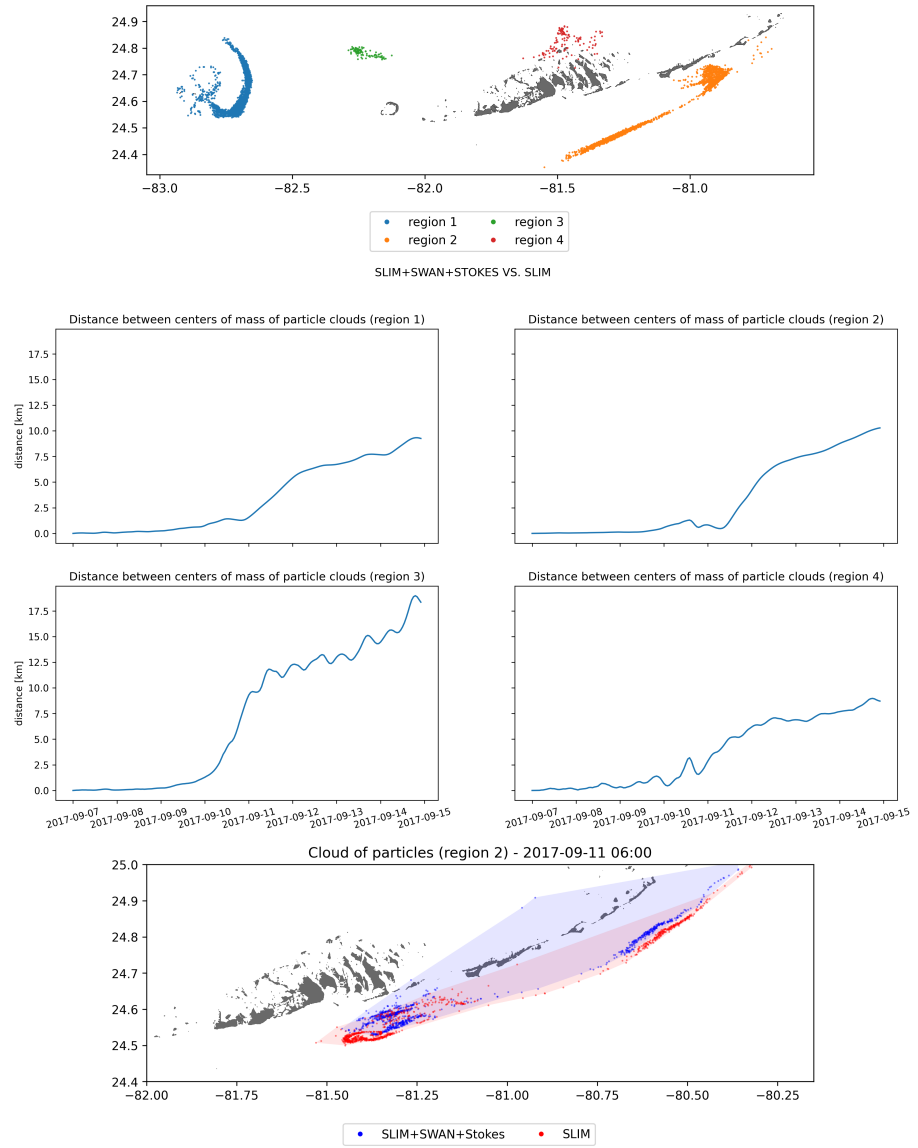


Fig. 7: Comparison of passive drifters trajectories with SLIM+SWAN+Stokes drift vs. SLIM alone. A snapshot of the positions of the particles released from region 2 is shown after the passage of Irma in the Florida Keys. Particles advected by the currents of the coupled model tend to remain on the shelf while particles advected by SLIM alone are mostly transported along the shelf break

267 Conflict of Interest Statement

268 The authors declare that the research was conducted in the absence of any
269 commercial or financial relationships that could be construed as a potential
270 conflict of interest.

271 Author Contributions

272 Funding

273 Acknowledgments

274 Computational resources were provided by the Consortium des Équipements
275 de Calcul Intensif (CÉCI), funded by the F.R.S.-FNRS under Grant No. 2.5020.11.
276 Thomas Dobbelaere is a PhD student supported by the Fund for Research
277 training in Industry and Agriculture (FRIA/FNRS).

278 Supplementary Material

279 The Supplementary Material for this article is attached to the submitted
280 document.

281 References

- 282 Booij, N., Ris, R. C., and Holthuijsen, L. H. (1999). A third-generation wave
283 model for coastal regions: 1. Model description and validation. *Journal*
284 *of geophysical research: Oceans*, 104(C4):7649–7666.
- 285 Chassignet, E. P., Hurlburt, H. E., Smedstad, O. M., Halliwell, G. R., Hogan,
286 P. J., Wallcraft, A. J., Baraille, R., and Bleck, R. (2007). The HYCOM
287 (hybrid coordinate ocean model) data assimilative system. *Journal of*
288 *Marine Systems*, 65(1-4):60–83.

- 289 Cowen, R. K. and Sponaugle, S. (2009). Larval dispersal and marine
290 population connectivity.
- 291 Dietrich, J., Westerink, J., Kennedy, A., Smith, J., Jensen, R., Zijlema, M.,
292 Holthuijsen, L., Dawson, C., Luettich, R., Powell, M., et al. (2011).
293 Hurricane gustav (2008) waves and storm surge: Hindcast, synoptic
294 analysis, and validation in southern Louisiana. *Monthly Weather Review*,
295 139(8):2488–2522.
- 296 Dobbelaere, T., Muller, E., Gramer, L., Holstein, D., and Hanert, E. (2020a).
297 Report on the potential origin of the SCTLD in the Florida Reef Tract.
298 Available online at: [https://floridadep.gov/rcp/coral/documents/
299 report-potential-origin-sctld-florida-reef-tract](https://floridadep.gov/rcp/coral/documents/report-potential-origin-sctld-florida-reef-tract).
- 300 Dobbelaere, T., Muller, E. M., Gramer, L. J., Holstein, D. M., and Hanert, E.
301 (2020b). Coupled epidemic-hydrodynamic modeling to understand the
302 spread of a deadly coral disease in Florida. *Frontiers in Marine Science*,
303 7:1016.
- 304 Donelan, M., Haus, B., Reul, N., Plant, W., Stiassnie, M., Gruber, H., Brown,
305 O., and Saltzman, E. (2004). On the limiting aerodynamic roughness of
306 the ocean in very strong winds. *Geophysical Research Letters*, 31(18).
- 307 Figueiredo, J., Baird, A. H., and Connolly, S. R. (2013). Synthesizing larval
308 competence dynamics and reef-scale retention reveals a high potential
309 for self-recruitment in corals. *Ecology*, 94(3):650–659.
- 310 Frys, C., Saint-Amand, A., Le Hénaff, M., Figueiredo, J., Kuba, A., Walker, B.,
311 Lambrechts, J., Vallaeyns, V., Vincent, D., and Hanert, E. (2020). Fine-
312 scale coral connectivity pathways in the Florida Reef Tract: implications
313 for conservation and restoration. *Frontiers in Marine Science*, 7:312.
- 314 Fujimura, A. G., Reniers, A. J., Paris, C. B., Shanks, A. L., MacMahan, J. H.,
315 and Morgan, S. G. (2014). Numerical simulations of larval transport into
316 a rip-channeled surf zone. *Limnology and Oceanography*, 59(4):1434–
317 1447.
- 318 Geuzaine, C. and Remacle, J.-F. (2009). Gmsh: A 3-d finite element mesh
319 generator with built-in pre-and post-processing facilities. *International
320 journal for numerical methods in engineering*, 79(11):1309–1331.

- 321 Harper, B., Kepert, J., and Ginger, J. (2010). *Guidelines for converting*
322 *between various wind averaging periods in tropical cyclone conditions.*
323 Citeseer.
- 324 Hegermiller, C. A., Warner, J. C., Olabarrieta, M., and Sherwood, C. R.
325 (2019). Wave-current interaction between Hurricane Matthew wave
326 fields and the Gulf Stream. *Journal of Physical Oceanography*,
327 49(11):2883–2900.
- 328 Hoffmeister, J. and Multer, H. (1968). Geology and origin of the Florida Keys.
329 *Geological Society of America Bulletin*, 79(11):1487–1502.
- 330 Holthuijsen, L. H., Powell, M. D., and Pietrzak, J. D. (2012). Wind and waves
331 in extreme hurricanes. *Journal of Geophysical Research: Oceans*,
332 117(C9).
- 333 Janssen, P. A. (1991). Quasi-linear theory of wind-wave generation applied
334 to wave forecasting. *Journal of physical oceanography*, 21(11):1631–
335 1642.
- 336 Johns, W. E. and Schott, F. (1987). Meandering and transport variations
337 of the Florida Current. *Journal of physical oceanography*, 17(8):1128–
338 1147.
- 339 Knaff, J. A., Sampson, C. R., and Musgrave, K. D. (2018). Statistical tropi-
340 cal cyclone wind radii prediction using climatology and persistence:
341 Updates for the western North Pacific. *Weather and Forecasting*,
342 33(4):1093–1098.
- 343 Komen, G., Hasselmann, S., and Hasselmann, K. (1984). On the exis-
344 tence of a fully developed wind-sea spectrum. *Journal of physical*
345 *oceanography*, 14(8):1271–1285.
- 346 Kourafalou, V. H. and Kang, H. (2012). Florida Current meandering and
347 evolution of cyclonic eddies along the Florida Keys Reef Tract: Are they
348 interconnected? *Journal of Geophysical Research: Oceans*, 117(C5).
- 349 Landsea, C. W. and Franklin, J. L. (2013). Atlantic hurricane database un-
350 certainty and presentation of a new database format. *Monthly Weather*
351 *Review*, 141(10):3576–3592.

- 352 Lee, T. N., Leaman, K., Williams, E., Berger, T., and Atkinson, L. (1995).
353 Florida Current meanders and gyre formation in the southern Straits
354 of Florida. *Journal of Geophysical Research: Oceans*, 100(C5):8607–
355 8620.
- 356 Lee, T. N. and Mayer, D. A. (1977). Low-frequency current variability and
357 spin-off eddies along the shelf off southeast Florida. *Collected Reprints*,
358 1(1):344.
- 359 Lee, T. N. and Smith, N. (2002). Volume transport variability through the
360 Florida Keys tidal channels. *Continental Shelf Research*, 22(9):1361–
361 1377.
- 362 Lee, T. N. and Williams, E. (1988). Wind-forced transport fluctuations of the
363 Florida Current. *Journal of Physical Oceanography*, 18(7):937–946.
- 364 Lidz, B. H. and Shinn, E. A. (1991). Paleoshorelines, reefs, and a rising sea:
365 South florida, usa. *Journal of Coastal Research*, pages 203–229.
- 366 Lin, N. and Chavas, D. (2012). On hurricane parametric wind and appli-
367 cations in storm surge modeling. *Journal of Geophysical Research: Atmospheres*, 117(D9).
- 369 Liu, Y. and Weisberg, R. H. (2012). Seasonal variability on the West Florida
370 shelf. *Progress in Oceanography*, 104:80–98.
- 371 Liu, Y., Weisberg, R. H., and Zheng, L. (2020). Impacts of hurricane Irma
372 on the circulation and transport in Florida Bay and the Charlotte Harbor
373 estuary. *Estuaries and Coasts*, 43(5):1194–1216.
- 374 Madsen, O. S., Poon, Y.-K., and Gruber, H. C. (1989). Spectral wave
375 attenuation by bottom friction: Theory. In *Coastal Engineering 1988*,
376 pages 492–504.
- 377 Mei, C. C. (1989). *The applied dynamics of ocean surface waves*, volume 1.
378 World scientific.
- 379 Moon, I.-J., Ginis, I., Hara, T., and Thomas, B. (2007). A physics-based
380 parameterization of air–sea momentum flux at high wind speeds and
381 its impact on hurricane intensity predictions. *Monthly weather review*,
382 135(8):2869–2878.

- 383 Pinelli, J.-P., Roueche, D., Kijewski-Correa, T., Plaz, F., Prevatt, D., Zisis,
384 I., Elawady, A., Haan, F., Pei, S., Gurley, K., et al. (2018). Overview
385 of damage observed in regional construction during the passage of
386 Hurricane Irma over the State of Florida. In *Forensic Engineering 2018: Forging Forensic Frontiers*, pages 1028–1038. American Society of
387 Civil Engineers Reston, VA.
388
- 389 Powell, M. D., Houston, S. H., Amat, L. R., and Morisseau-Leroy, N. (1998).
390 The HRD real-time hurricane wind analysis system. *Journal of Wind
391 Engineering and Industrial Aerodynamics*, 77:53–64.
- 392 Powell, M. D., Vickery, P. J., and Reinhold, T. A. (2003). Reduced drag coefficient
393 for high wind speeds in tropical cyclones. *Nature*, 422(6929):279–
394 283.
- 395 Schott, F. A., Lee, T. N., and Zantopp, R. (1988). Variability of structure and
396 transport of the Florida Current in the period range of days to seasonal.
397 *Journal of Physical Oceanography*, 18(9):1209–1230.
- 398 Shinn, E. A. (1988). The geology of the Florida Keys. *Oceanus*, 31(1):46–53.
- 399 Siadatmousavi, S. M., Jose, F., and Stone, G. (2011). Evaluation of two WAM
400 white capping parameterizations using parallel unstructured SWAN
401 with application to the Northern Gulf of Mexico, USA. *Applied Ocean
402 Research*, 33(1):23–30.
- 403 Tolman, H. L. et al. (2009). User manual and system documentation of
404 WAVEWATCH III TM version 3.14. *Technical note, MMAB Contribution*,
405 276:220.
- 406 Villas Bôas, A. B., Cornuelle, B. D., Mazloff, M. R., Gille, S. T., and Arduin,
407 F. (2020). Wave–current interactions at meso-and submesoscales:
408 Insights from idealized numerical simulations. *Journal of Physical
409 Oceanography*, 50(12):3483–3500.
- 410 Weisberg, R., Liu, Y., and Mayer, D. (2009). Mean circulation on the west
411 Florida continental shelf observed with long-term moorings. *Geophys.
412 Res. Lett.*, 36:L19610.
- 413 Xian, S., Feng, K., Lin, N., Marsooli, R., Chavas, D., Chen, J., and Hatzikyri-
414 akou, A. (2018). Brief communication: Rapid assessment of damaged

415 residential buildings in the Florida Keys after Hurricane Irma. *Natural*
416 *Hazards and Earth System Sciences*, 18(7):2041–2045.

417 Zhang, C., Durgan, S. D., and Lagomasino, D. (2019). Modeling risk of man-
418 groves to tropical cyclones: A case study of Hurricane Irma. *Estuarine,*
419 *Coastal and Shelf Science*, 224:108–116.